ADVANCED MATERIALS INTERFACES
www.advmatinterfaces.de

Increasing the Strength, Hardness, and Survivability of Semiconducting Polymers by Crosslinking

*Alexander X. Chen, Jeremy D. Hilgar, Anton A. Samoylov, Silpa S. Pazhankave, Jordan A. Bunch, Kartik Choudhary, Guillermo L. Esparza, Allison Lim, Xuyi Luo, Hu Chen, Rory Runser, Iain McCulloch, Jianguo Mei, Christian Hoover, Adam D. Printz, Nathan A. Romero, and Darren J. Lipomi**

Crosslinking is a ubiquitous strategy in polymer engineering to increase the thermomechanical robustness of solid polymers but has been relatively unexplored in the context of π-conjugated (semiconducting) polymers. Notwithstanding, mechanical stability is key to many envisioned applications of organic electronic devices. For example, the wide-scale distribution of photovoltaic devices incorporating conjugated polymers may depend on integration with substrates subject to mechanical insult—for example, road surfaces, flooring tiles, and vehicle paint. Here, a four-armed azide-based crosslinker ("4Bx") is used to modify the mechanical properties of a library of semiconducting polymers. Three polymers used in bulk heterojunction solar cells (donors J51 and PTB7-Th, and acceptor N2200) are selected for detailed investigation. In doing so, it is shown that low loadings of 4Bx can be used to increase the strength (up to 30%), toughness (up to 75%), hardness (up to 25%), and cohesion of crosslinked films. Likewise, crosslinked films show greater physical stability in comparison to non-crosslinked counterparts (20% vs 90% volume lost after sonication). Finally, the locked-in morphologies and increased mechanical robustness enable crosslinked solar cells to have greater survivability to four degradation tests: abrasion (using a sponge), direct exposure to chloroform, thermal aging, and accelerated degradation (heat, moisture, and oxygen).

1. Introduction

π-Conjugated polymers exhibit the electronic functionality of conductors and semiconductors. Ideally, they would also have the mechanical robustness of engineering plastics, as the mechanical properties of semiconducting polymers are a crucial determinant for device applications. However, the majority of research on the mechanical properties of semiconducting polymers has been focused on increasing the parameters associated with "softness"— that is, low modulus and high fracture strain.[1] This focus has been primarily driven by an interest in stretchable devices, such as flexible thin-film transistors, solar cells, and sensors. The emphasis on increasing the softness is incompatible with a number of compelling applications for semiconducting polymers, in which strength and hardness are desirable. For example, thin-film solar cells integrated with rooftops, roads, sidewalks, parking lots, and vehicle and aeronautic surfaces;

A. X. Chen, J. A. Bunch, K. Choudhary, G. L. Esparza, A. Lim, R. Runser, D. J. Lipomi
Department of Nanoengineering
University of California, San Diego
9500 Gilman Dr. Mail Code 0448, La Jolla, CA 92093, USA
E-mail: dlipomi@eng.ucsd.edu

J. D. Hilgar, N. A. Romero
Department of Chemistry and Biochemistry
University of California, San Diego
9500 Gilman Dr. Mail Code 0332, La Jolla, CA 92093-0448, USA

A. A. Samoylov, A. D. Printz
Department of Chemical and Environmental Engineering
University of Arizona
Tucson, AZ 85721, USA

The ORCID identification number(s) for the author(s) of this article can be found under https://doi.org/10.1002/admi.202202053.

DOI: 10.1002/admi.202202053

S. S. Pazhankave, C. Hoover
School of Sustainable Engineering and the Built Environment
Arizona State University
Tempe, AZ 85287, USA

G. L. Esparza
Materials Science and Engineering Program
University of California, San Diego
9500 Gilman Dr. Mail Code 0418, La Jolla, CA 92093, USA

X. Luo, J. Mei
Department of Chemistry
Purdue University
West Lafayette, IN 47907, USA

H. Chen
King Abdullah University of Science and Technology (KAUST)
Physical Science and Engineering Division
Thuwal 23955–6900, Saudi Arabia

I. McCulloch
Department of Chemistry
University of Oxford
Oxford OX1 3TA, UK

heads-up displays in eyeglasses, windshields, and cockpits; and integration with textiles, especially in physically demanding contexts (military, rescue, and medical workers). Here, we examine the use of a four-armed azide-containing crosslinker as a means of increasing the hardness, strength, and cohesive energy of a library of conjugated polymers. This material, the previously reported "4Bx,"[2] works by crosslinking the aliphatic side chains of the polymer. From this library, we select three which are promising for organic bulk heterojunction solar cells. By measuring the performance of these devices, we determine that it should be possible to increase the robustness of previously reported and commercially available materials.

There are many approaches to modulating the mechanical properties of solid films of conjugated polymers. These approaches range from physical blending[3–12] to chemical modification and re-engineering of the backbone and side chains.[1,4,6,13–15] One approach, which is well-known in polymer engineering yet less explored in the field of conjugated polymers, is crosslinking. In their pioneering work, Kim et al. showed that a four-armed perfluorophenyl azide crosslinker (4Bx) could be used to crosslink a diketopyrrolopyrrole (DPP)-based polymer (by enabling solvent orthogonality) to fabricate arrays of all-photopatterned organic transistors.[2] Moreover, the authors showed that low loadings (1 wt%) of 4Bx could increase the strength, toughness, and fracture strain of a crosslinked DPP polymer film without decreasing the charge-carrier mobility. Likewise, work by Zheng et al. showed that crosslinking can yield films with high intrinsic elasticity. Stretchable semiconducting matrices were formed by crosslinking diketopyrrolopyrrole-based or indacenodithiophene-based polymers (i.e., IDTBT) using a perfluorophenyl azide end-capped polybutadiene crosslinker.[16] By crosslinking IDTBT in a rubber matrix, Zheng et al. were able to produce ultrathin films with an intrinsic elasticity of 70%, which could maintain hole mobilities of 1 $cm^2\ V^{-1}\ s^{-11}$ after 1000 cycles of stretching to 50% strain.

Likewise, the Anthopoulos group has shown that the chemical structure of the crosslinker plays an important role in determining the mechanical properties.[17] For example, Dauzon et al. crosslinked fullerene acceptors in P3HT:PCBM bulk heterojunctions using three bisazide crosslinkers: 1,12-diazidododecane ($C_{12}N_3$), 1,11-diazido-3,6,9-trioxaundecane (PEG_3N_3), and poly(ethylene glycol) bisazide (PEG_NN_3).[17] Increasing the crosslinker loading and increasing the carbon chain length of the crosslinker both resulted in a decrease in the elastic modulus. Encouragingly, the authors also showed that small loadings of crosslinker (5 wt%) could be incorporated in a P3HT:PCBM solar cell without reducing the power conversion efficiency (PCE). Similarly, work from the Shao group showed that 2,6-bis(4-azidobenzylidene)cyclohexanone (BAC) could be used to crosslink PM6, a benzodithiophene-based low-bandgap polymer.[18] Increasing the BAC loading in crosslinked PM6 films resulted in a continuous increase in mechanical robustness (e.g., fracture strain, tensile strength, and toughness). At 10 wt% BAC, the crosslinked PM6 film showed a significant increase in the plastic regime, resulting in an increased fracture strain (5% vs 20%), tensile strength (30 vs 50 MPa), and toughness (≈0.5 vs 8 MJ m^{-3}) compared to a non-crosslinked PM6 film. Thus, the crosslinker structure and loading are significant determinants of both the mechanical and electronic properties of the active layer in an organic solar cell (OSC).

In addition to increasing the mechanical robustness, crosslinking may also stabilize the morphology of a bulk heterojunction solar cell and increase the lifespan of the device. A significant body of this literature focuses on crosslinking polymer-fullerene blends using a variety of strategies, as have been discussed by Rumer and McCulloch.[19] In most of this work, the crosslinking process is non-selective (e.g., can occur between polymer/polymer, polymer/fullerene, and fullerene/fullerene).[20] While increased lifespan and thermal stability of crosslinked devices often come at the cost of a lower initial PCE,[19] this trade-off is not guaranteed.[20–23] For example, Hong et al. have shown that crosslinking a fullerene derivative (PCBSD) in a tertiary bulk heterojunction with a benzodithiophene-based donor and a fused-ring electron acceptor (PBDBTF:Y6:*c*-PCBSD) can increase the PCE from 15.1% to 16.1% while improving device stability.[21] In spite of the foundational work on polymer-fullerene devices, there is significant interest in both all-polymer[24–26] blends and non-fullerene acceptors.[27–30] Some of this arises from the presumed superior mechanical reliability of all-polymer blends[1,31,32] and the high PCEs enabled by non-fullerene acceptors.[33,34] In three studies,[35–37] authors showed that crosslinked bulk heterojunction films containing D–A polymers outperformed their non-crosslinked counterparts in both PCE and device stability.

In this work, we used 4Bx as a crosslinker for a library of 11 semiconducting polymers (spanning a wide range of chemical structures) as a means of increasing mechanical robustness. The azide moiety of 4Bx undergoes C–H insertion in the presence of heat or UV light,[2,38] thus rendering this crosslinking strategy universal for all polymers with aliphatic side chains. A subset of the polymers tested was selected for use in two all-polymer bulk heterojunction solar cells. Both blends incorporate a poly(naphthalene diimide) derivative (N2200) as the acceptor polymer and a benzodithiophene (BDT)-derivative as a donor polymer (J51, PTB7-Th). In doing so, we elucidate how crosslinking modulate the mechanical properties of semiconducting polymer films, as well as how crosslinking affects the mechanical and electronic properties of all-polymer bulk heterojunctions for OSC applications.

2. Experimental Section

2.1. Selection of Materials

For this study, the effect of crosslinking on a library of eleven semiconducting polymers: DPP-C3,[39] DPP-C9,[39] PTB7, PTB7-Th, J51, P3HpT, TQ1, IDTBT,[40,41] 2DPP-2CNTVT,[42] N2200, and PZ1 was investigated.[43] For solar cells, two donor polymers (PTB7-Th, J51) and one acceptor polymer (N2200) comprising two different bulk heterojunctions, J51:N2200 and PTB7-Th:N2200 were selected. The two selected polymer blends had similar benzodithiophene (BDT)-based donor polymers that paired with N2200 as the acceptor. These polymer blends were selected because the recipes for such devices were well-documented in the existing literature.[44,45] Likewise, the ratios of the donor to acceptor polymer for J51:N2200 (1:2)[44] and

PTB7-Th:N2200 (2:1)[45] were chosen from existing literature. Similarly, recipes with different ratios were chosen to elucidate how the composition of the bulk heterojunction (e.g., whether it contained more p-type or n-type material) would change the effect of crosslinking. As the crosslinker, (2,2-bis(((4-azido2,3,5,6-tetrafluorobenzoyl)oxy)methyl)propane-1,3-diyl bis(4-azido-2,3,5,6-tetrafluorobenzoate) (4Bx) was used, which was reactive toward the aliphatic side chains of nearly all conjugated polymers. Previous work suggested that 4Bx could be used to crosslink isolated polymers at low loadings with no loss in mobility.[2] It was reasoned that 4Bx could possibly be applied to crosslink bulk heterojunctions (i.e., polymer blends) without severe inhibition of the photovoltaic properties.

2.2. Mechanical Testing

To determine the tensile behavior of the films, a pseudo-free-standing tensile testing method (i.e., film-on-water, FOW) was used.[1,46] The compressive properties (e.g., modulus, hardness) of crosslinked and non-crosslinked polymer films were measured from nanoindentation[47–55] using the Oliver–Pharr method[56] (with an approximation of the Poisson ratio[57]). Finally, a cohesive fracture test was done using a double cantilever beam (DCB) setup[58] in order to determine the energy required to propagate a crack along that interface (G_C). Following a fracture, X-ray photoelectron spectroscopy (XPS) was used to determine the interface at which the device stack fractured.

2.3. Solar Cells

The solar cells were fabricated in order to directly probe physical changes within the bulk heterojunction. In these bulk heterojunction films, 1,8-diiodooctane (DIO) was added, which was commonly used to make the morphology of the solid film more amenable to charge separation and transport. Residual DIO in the bulk heterojunction acted as a photoacid that was harmful to the photovoltaic properties,[59,60] and was removed by annealing at an elevated temperature (175 °C for 1 h). Instead of using top contacts based on evaporated metal, it was elected to use eutectic gallium indium (EGaIn).[61] The use of removable drops of liquid EGaIn, while not practical for large-area devices, made it possible to measure the properties of underlying conjugated polymer films before and after photovoltaic measurements (e.g., without degradation at a polymer-metal interface for devices with evaporated contacts). This decision was made fully aware that the performance metrics of the resulting "devices" would be lower than they would be with evaporated contacts.

2.4. Degradation Testing

Several degradation tests were performed to understand how crosslinking with 4Bx affects the physical performance of J51:N2200 and PTB7-Th:N2200 blends. Accelerated degradation tests were conducted by 1) annealing solar cells at 60 °C and 2) aging solar cells in a 50 °C, 50% relative humidity chamber. Likewise, the solvent resistance of the crosslinked active layer was evaluated by immersion of solar cells in chloroform. Finally, the abrasion resistance was evaluated in two ways. First, a bath sonicator was used to physically abrade polymer films using high-frequency sound waves in water. Second, the scouring (rougher) surface of a dish sponge was used to abrade the bulk heterojunction films when incorporated into photovoltaic devices.

2.5. Morphological Characterization

Fourier-transform infrared (FTIR) spectroscopy was used to qualitatively observe the crosslinking of 4Bx in conjugated polymer films. Crosslinking was verified by reduction of the azide peak (2160–2120 cm^{-1}) using FTIR (Figure S1, Supporting Information). UV–vis spectroscopy was used to determine, 1) the change in thickness in polymer films during sonication abrasion tests and 2) the change in aggregation[62] (e.g., short-range order) in crosslinked and non-crosslinked poly(3-heptylthiophene) (P3HpT) films (Figure S2, Supporting Information). P3HpT was used as a proxy polymer because the aggregation behavior of poly(3-alkylthiophene)s had been extensively studied by Spano and coworkers.[62,63]

3. Results and Discussion

The library of polymers investigated in this work differed greatly in chemical structure (**Figure 1**) and morphology, both of which can possibly affect the crosslinking (and thus mechanical properties) of the solid film. Particular attention was given to diketopyrrolopyrrole (DPP)-based (e.g., DPP-C3, DPP-C9, and 2DPP-2CNTVT) and benzodithiophene (BDT)-based polymers (e.g., PTB7, PTB7-Th, J51), which are motifs common to the design and synthesis of semiconducting polymers used for both solar cells and transistors. Within each family, these polymers differ primarily in terms of backbone structure, the electronegativity of donor-acceptor moieties, and backbone rigidity. Most polymers used are semi-crystalline (e.g., DPP-based and BDT-based materials), apart from the inclusion of IDTBT and TQ1, which are primarily amorphous (e.g., with low crystallinity). Detailed studies elucidating the morphology of each polymer can be found elsewhere.[39,42,70–72,43,45,64–69]

For all 11 polymers, the addition of 1 wt% 4Bx as a crosslinker resulted in an increase in the ultimate tensile strength, toughness, and resilience of the solid film, as determined by tensile testing of pseudo-free-standing films (**Figure 2**a,b,e). In most cases, crosslinking also resulted in a similar or greater fracture strain and linear elasticity compared to the non-crosslinked film (Figure 2c,f). These findings are consistent with previous results in which the tensile properties of a DPP-based polymer were studied,[2] and can generally be attributed to the greater amounts of energy dissipation allowed by the crosslinks formed at the optimal 1 wt% loading. However, the elastic modulus between crosslinked and non-crosslinked conjugated polymers remained similar (Figure 2d). One of the most significant differences was between the tensile behavior

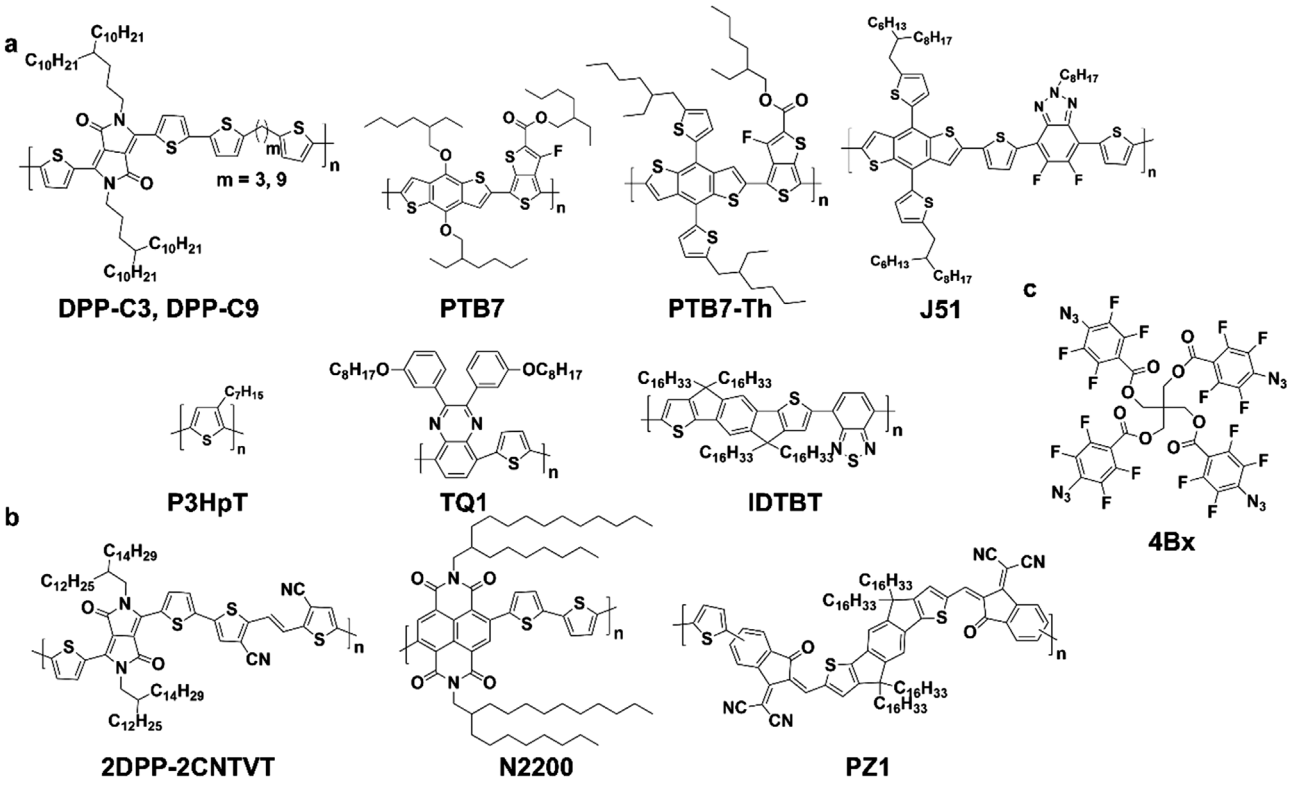

Figure 1. The a) p-type and b) n-type semiconducting polymers and c) crosslinker ("4Bx") were used in this study.

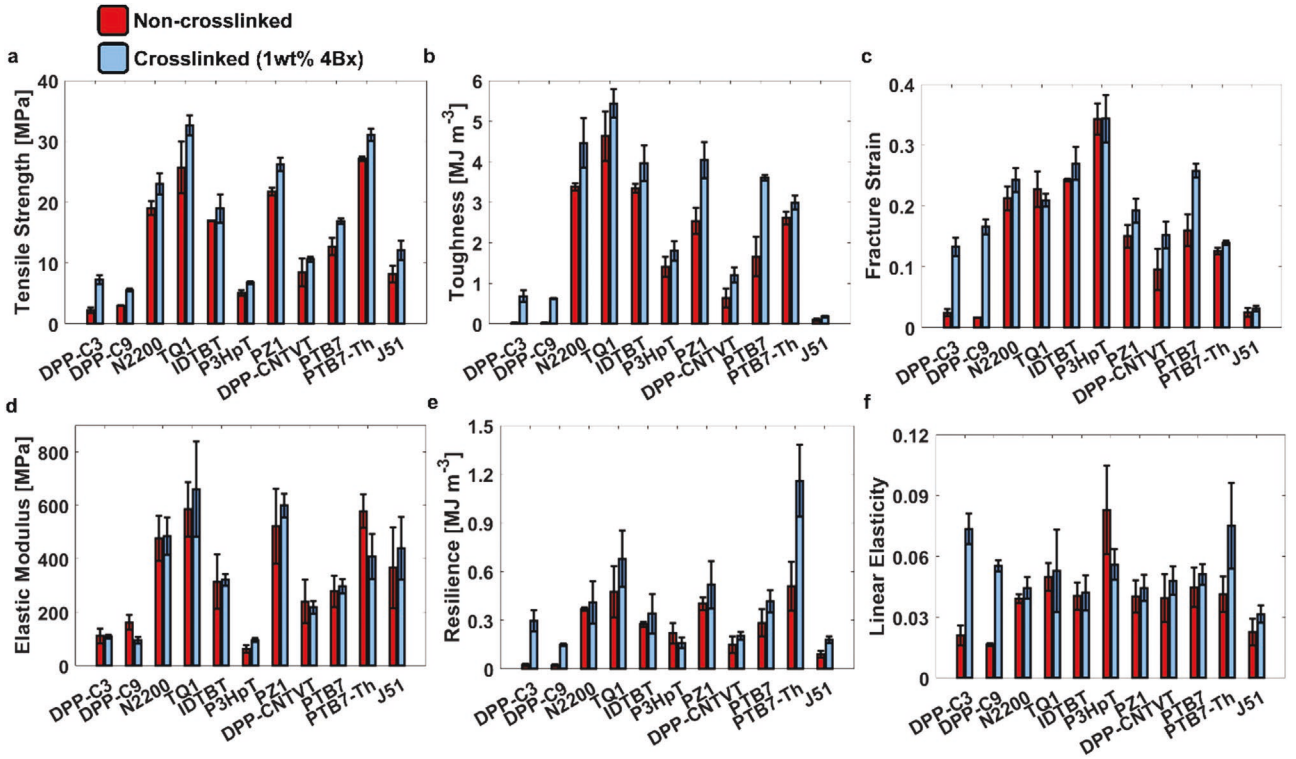

Figure 2. Mechanical properties of interest were extracted from stress-strain curves produced by tensile tests of 11 semiconducting polymers. Differences between non-crosslinked (red) polymers and polymers crosslinked with 1 wt% 4Bx (blue) are shown for a) tensile strength, b) toughness, c) fracture strain, d) elastic modulus, e) resilience, and f) linear elasticity.

of the non-crosslinked and crosslinked DPP-C3 and DPP-C9 films. With the lowest molecular weight (M_n ≈9.4 kDa, Section S1.3, Supporting Information), non-crosslinked DPP-C3 was extremely brittle with low tensile strength, toughness, and fracture strain. Crosslinking with 4Bx greatly increased the values of these properties (along with the resilience and linear elasticity), likely due to an increase in the effective degree of polymerization and entanglement density. The same was true for DPP-C9, which had the second lowest molecular weight (M_n ≈13.9 kDa, Section S1.3, Supporting Information). In contrast, crosslinking PTB7 (the second highest molecular weight polymer studied, with an M_n ≈83 kDa, Section S1.3, Supporting Information) resulted primarily in an increase in the fracture strain. Coupled with the small increase in tensile strength, this increase in the extensibility resulted in a significant increase in the toughness of the crosslinked film. Interestingly, crosslinked PTB7-Th films showed only a small increase in the overall mechanical robustness (i.e., tensile strength, toughness, and fracture strain), but resulted in a significantly greater resilience due to the increased range of linear elasticity. Thus, the manner in which crosslinking with 4Bx affects the tensile properties of a semiconducting polymer film is also dependent on chemical structure and molecular characteristics (e.g., degree of polymerization, the density of entanglements).

From this library, we selected three polymers common in the field of organic photovoltaics to incorporate in the bulk heterojunction of OSCs. Devices were fabricated with two different blends: J51:N2200 (1:2)[42] and PTB7-Th:N2200 (2:1).[45] To elucidate how crosslinking affects the mechanical properties of each blend, film-on-water (FOW) tensile tests were conducted on J51:N2200 and PTB7-Th:N2200 films with varied 4Bx loadings (**Figure 3**). We observed somewhat different effects of crosslinking for the two different blends. For J51:N2200, as the 4Bx loading increased from 0 wt% to 1 wt%, the strength, modulus, toughness, and fracture strain all increased. A further increase in 4Bx loading to 2 wt% slightly embrittled the film and decreased the fracture strain, but the strength of the film was increased further. However, at 2 wt%, the crosslinked film showed greater tensile strength at the expense of the fracture strain (0.086), which was less than that of the non-crosslinked film (0.12). Therefore, for J51:N2200, our findings suggest that 1 wt% 4Bx can be incorporated to optimize the fracture strain while increasing the strength and toughness. In contrast, there was a clear mechanical trade-off for PTB7-Th:N2200 relative to increasing crosslinker loading. Increasing the loading of 4Bx generally resulted in increased strength but decreased fracture strain.

The two types of blends differ in two aspects: the chemical structure of the donor polymer, and the ratio of donor to acceptor polymer (derived from the literature for giving the optimized device performance[44,45]). The extracted tensile properties for all polymers and polymer blends are shown in Table S1, Supporting Information. For all three neat polymers (Figure S3, Supporting Information), crosslinking with 1 wt% 4Bx resulted in an increase in the fracture strain and tensile strength (though J51 failed by brittle fracture while PTB7-Th

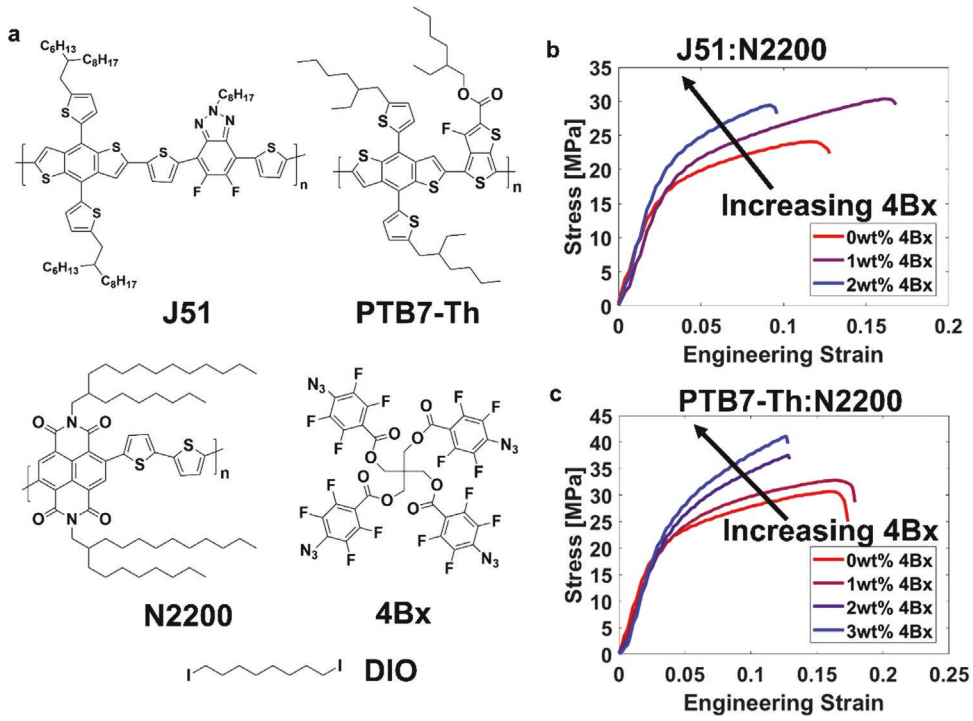

Figure 3. a) Chemical structures of J51, PTB7-Th, N2200, 4Bx, and DIO. J51 and PTB7-Th are used as the donor polymers in a bulk heterojunction with N2200, an acceptor polymer. DIO is added as a small molecule additive to improve the morphology for each bulk heterojunction. 4Bx is added to each bulk heterojunction as a crosslinker. Pseudo-free standing tensile tests are conducted on b) 12 mg mL^{-1} (1:2) J51:N2200 (3 vol% DIO) and c) 12 mg mL^{-1} (2:1) PTB7-Th:N2200 (2 vol% DIO) thin films to measure the tensile response. Films are annealed at 175 °C for 60 min in order to initiate crosslinking and remove residual DIO. Representative stress-strain curves are shown in (b,c).

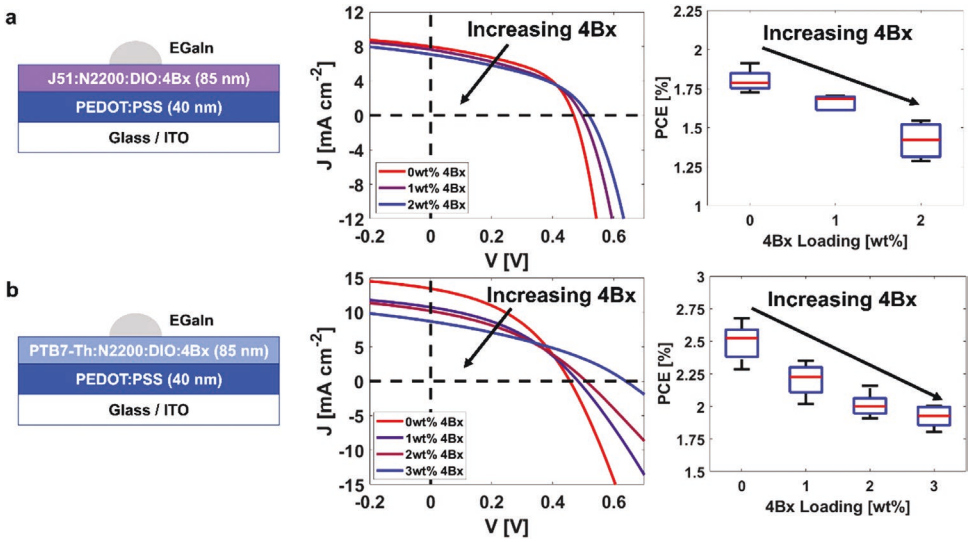

Figure 4. Photovoltaic properties of EGaIn solar cells with a) J51:N2200 and b) PTB7-Th:N2200 bulk heterojunctions relative to increasing 4Bx loading. Device structure and representative inverted *J–V* curves are shown for each bulk heterojunction, along with the change in power conversion efficiency (PCE) relative to 4Bx loading. The red lines in the boxplots represent the average PCE for each loading of 4Bx. A total of six EGaIn measurements were made on each device.

and N2200 failed by ductile fracture). Additionally, crosslinked films of J51 were stiffer (i.e., a greater elastic modulus) than their non-crosslinked counterparts. In PTB7-Th and N2200, crosslinking primarily resulted in a drawn-out plastic regime prior to fracture, and a corresponding increase in toughness. In the elastic regime, both PTB7-Th and N2200 also showed similar behaviors. Crosslinking with 4Bx resulted in an extension of the elastic regime (i.e., linear elasticity, resilience, and yield stress) of the film with little difference in modulus.

In the J51:N2200 bulk heterojunction, one significant observation is the ductile behavior, despite the apparent brittleness of J51 on its own. This plastic behavior is likely due to the relatively high loading of N2200 (1:2 ratio) in the polymer blend (as well as an increased density of entanglements from the blending of two polymers[73–75]). Similar to the isolated ductile polymers, crosslinking J51:N2200 with 1 wt% 4Bx generally resulted in the same changes to the plastic regime: greater fracture strain, greater tensile strength, and greater toughness. The modulus remained similar to the non-crosslinked film but increased when the 4Bx loading was increased to 2 wt%. Interestingly, the PTB7-Th:N2200 blend with 1 wt% 4Bx showed similar tensile behavior to the J51:N2200 counterpart. Further addition of 4Bx (up to 3 wt%) resulted in a monotonic increase in both the tensile strength and the modulus of the polymer film. Notably, in both J51:N2200 and PTB7-Th:N2200, the tensile strength of the crosslinked blend was greater than that of any isolated polymer. Again, this effect can likely be attributed to the greater entanglement density within a polymer blend.[73–75]

To elucidate how crosslinking affects the photovoltaic properties of the two bulk heterojunctions, we fabricated solar cells with the architecture shown in **Figure 4**. For both J51:N2200 and PTB7-Th:N2200 devices, we find that an increase in 4Bx loading generally corresponded to lower J_{sc} and FF, which resulted in a lower PCE. This change in photovoltaic behavior was due to an increase in series resistance. Likewise, the addition of 4Bx also resulted in an increased V_{oc}, although this was not sufficient to offset the PCE lost in either bulk heterojunction. Additionally, crosslinked PTB7-Th:N2200 devices without DIO showed a greater decrease in electronic performance when compared to devices containing DIO, largely due to a greater decrease in FF (Figure S4, Supporting Information). This comparison suggests that the increased V_{oc} is possibly due to changes in the chemical composition of the bulk heterojunction with the addition of both DIO and 4Bx. It is possible that small amounts of DIO remained crosslinked in the bulk heterojunction without being removed. These results validate prior studies suggesting that the incorporation of an azide-mediated crosslinker into the bulk heterojunction of an organic solar cell can result in a decreased initial PCE.[19] UV–vis of a proxy polymer, poly(3-heptylthiophene) (P3HpT), suggested that crosslinking with 4Bx decreases the short-range order (i.e., aggregation) of the polymer film, which possibly contributes to the decreased electronic performance (Figure S2, Supporting Information).

We demonstrate that crosslinking the bulk heterojunction increases the survivability of the solar cell for four different degradation tests (**Figure 5**). First, we show that the increased mechanical robustness of a crosslinked J51:N2200 bulk heterojunction can increase the survivability of solar cells subject to physical (e.g., scratch and abrasion) damage (Figure 5a, and Figure S5, Supporting Information). Second, we show that the insolubility of a crosslinked PTB7-Th:N2200 bulk heterojunction increases the resistance to organic solvents, even when directly exposed to chloroform (Figure 5b and Figure S6, Supporting Information). Third, to evaluate the thermal stability of crosslinked J51:N2200 cells, we subjected devices to thermal aging at 60 °C for 400 h in a nitrogen environment (Figure 5c and Figure S7, Supporting Information). Finally, we accelerate the degradation of PTB7-Th:N2200 solar cells using heat (50 °C), moisture (50% relative humidity), and oxygen

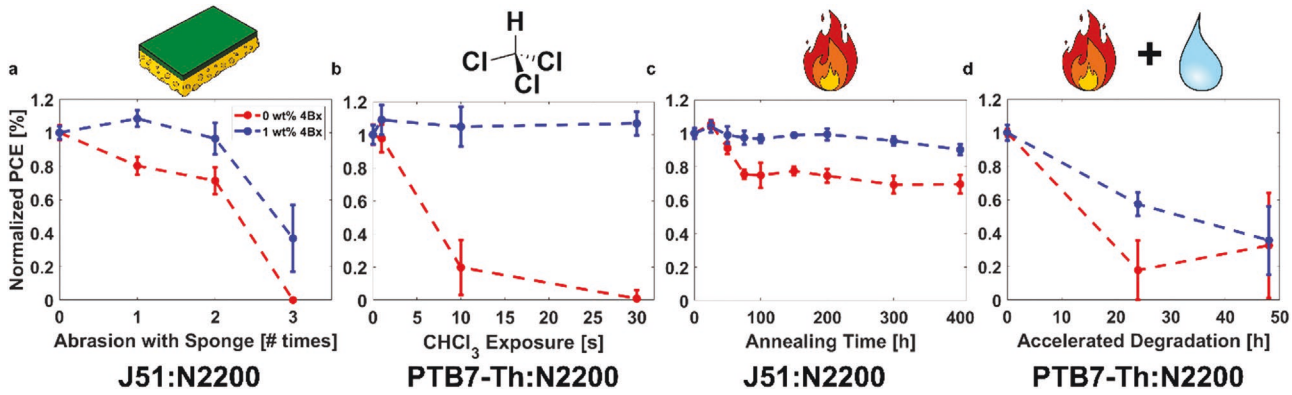

Figure 5. Normalized power conversion efficiencies of crosslinked and non-crosslinked EGaIn solar cells subject to a) abrasion tests using a sponge, b) direct exposure to chloroform, c) thermal aging at 60 °C, and d) accelerated degradation in atmospheric conditions at 50 °C and 50% relative humidity.

(e.g., in atmospheric conditions, with unencapsulated devices) (Figure 5d, and Figure S8, Supporting Information). The mechanisms by which water, heat, and oxygen accelerate degradation in OSCs have been investigated by others.[76–78] Detailed photovoltaic properties and *J*–*V* curves for each degradation test and all crosslinker loadings can be found in Figures S5–S8, Supporting Information.

Non-crosslinked films of semiconducting polymers can be easily damaged by relatively innocuous forces. That is, many semiconducting polymer films can be removed from a substrate by rubbing with a gloved finger. We used the abrasive side of a standard kitchen sponge (loaded with a 20 g weight to ensure contact) to gradually damage crosslinked and non-crosslinked J51:N2200 solar cells. We measured the photovoltaic properties every time the sponge was dragged over the film using a linear actuator. As expected, crosslinked solar cells showed greater survivability than their non-crosslinked counterparts. After both cells were abraded once, the crosslinked device showed little change in photovoltaic performance, with a similar J_{sc} and PCE to the pristine device (Figure 5a and Figure S5, Supporting Information). In comparison, the non-crosslinked device showed noticeably lower PCE due to the decreased J_{sc}. From optical microscopy, we observed many scratches on the active layer of the non-crosslinked device (Figure S9, Supporting Information). Although some scratches were present on the crosslinked J51:N2200 device, these were fewer and smaller. The non-crosslinked device failed after three abrasion cycles (short circuit, Figure S5, Supporting Information), at which point the crosslinked device still remained functional.

In addition to the locked morphology, crosslinking renders the bulk heterojunction insoluble to organic solvents. To demonstrate the increased solvent resistance of crosslinked bulk heterojunction films, PTB7-Th:N2200 cells were fabricated and directly exposed to chloroform. When the non-crosslinked device was dipped in chloroform, the active layer dissolved, resulting in the J_{sc}, V_{oc}, FF, and PCE monotonically decreasing until the active layer was completely removed (Figures S6 and S10, Supporting Information). In contrast, crosslinked bulk heterojunctions showed little change in photovoltaic performance. Exposure of the crosslinked bulk heterojunctions to chloroform for approximately 1 s dissolved any remaining non-crosslinked polymer and crosslinker, resulting in a small change in photovoltaic properties. After that initial change, all three crosslinked bulk heterojunctions (1–3 wt% 4Bx) remained highly resistant to the chloroform treatment and unchanged in terms of photovoltaic properties for immersions of up to 30 s.

Other studies have suggested that crosslinking the active layer of an OSC increases the thermal stability of the device.[19] Thus, we fabricated J51:N2200 cells and thermally aged crosslinked and non-crosslinked devices at 60 °C. Previous studies have shown that short annealing is beneficial for improving the crystallization, and thus charge transport, of bulk heterojunction films.[76] However, continuous heating may have the opposite effect in that it drives the morphology of the bulk heterojunction towards thermodynamic equilibrium (i.e., as opposed to a metastable morphology most favorable to charge transport).[76] In polymer:fullerene blends, previous studies have suggested that thermal aging results in greater phase separation.[77,79,80] As a result, larger polymer and fullerene domains are formed, reducing the effective surface area of donor-acceptor interfaces and reducing charge transfer.[79]

In the non-crosslinked J51:N2200 device, gradual annealing over 400 h resulted in significant changes in the photovoltaic properties of the bulk heterojunction (Figure 5c). The non-crosslinked device only maintained 68% of PCE after 400 h. In comparison, the 1 wt% 4Bx crosslinked device maintained ≈100% of its PCE over 200 h and 94% of its PCE over 400 h. Similarly, the device crosslinked with 2 wt% 4Bx maintained 100% of its PCE over 400 h. Previous studies have suggested that an Arrhenius model could relate accelerated thermal aging to the expected lifespan of the device at room temperature.[81] For P3HT:PCBM, aging a device for 200 h at 60 °C approximately corresponds to a lifespan of 1000 h at 25 °C.[81] Using this model, our findings suggest that the 1 wt% J51:N2200:4Bx bulk heterojunction would show no change in overall PCE for ≈1000 h at room temperature, while the 2 wt% bulk heterojunction would show no change for ≈2000 h.

Finally, PTB7-Th:N2200 devices were subjected to accelerated degradation conditions in a purpose-built chamber held at 50 °C and 50% relative humidity (RH) in the atmosphere. Devices were tested every 24 h and showed significant changes in the photovoltaic performance (Figure 5d). All cells showed significantly worsened photovoltaic properties after 24 h. Diagnostically, photovoltaic properties were worsened

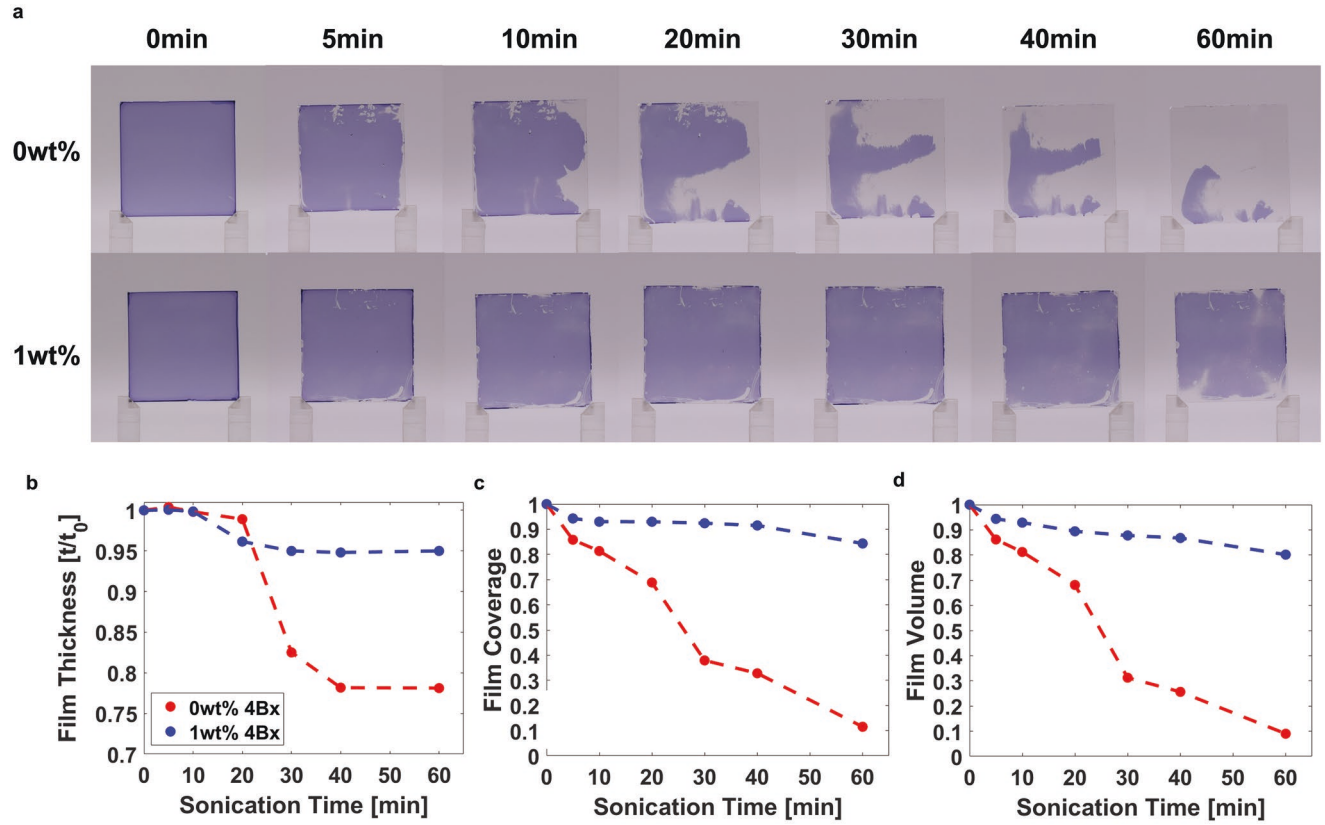

Figure 6. a) Crosslinked and non-crosslinked J51:N2200 films were sonicated in a bath sonicator for 1 h. Photographs of the films were taken periodically in order to compare the damage from physical agitation to the crosslinked and non-crosslinked films. Likewise, UV–vis measurements were taken of non-crosslinked crosslinked J51:N2200 films after each time interval of sonication. The absorbance peak at ≈390 nm for each spectrum was used to determine b) the change in film thickness relative to sonication time (for regions on the glass substrate where the film remained). Photographs of each film were taken after each time interval in order to approximate the c) surface area of the film using color thresholding. These changes in film thickness and surface area were used to approximate d) the total volume of the film removed due to agitation from the bath sonicator.

due to increased series resistance and failure was observed to occur by shunting (Figure S8, Supporting Information). This behavior was likely due to the degradation of the PEDOT:PSS, which is partially solubilized in the presence of water.[82,83] It is likely this ingress of moisture resulted in physical degradation (e.g., delamination of the ITO/PEDOT:PSS interface or PEDOT:PSS/PTB7-Th:N2200 interface) that resulted in increased series resistance (and shunting). Crosslinking with 2% 4Bx impeded this ingress, and thus the crosslinked device lasted longer. Thus, the observed changes to the photovoltaic properties of these devices were most likely a consequence of the degradation of the PEDOT:PSS layer. For example, the 3 wt% device completely shunted after 48 h in the degradation chamber, likely because the device was placed closest to the water vapor inlet. However, the non-crosslinked device was placed on the row furthest away from the water vapor valve (along with the 1 and 2 wt% devices), yet still showed the worst performance after 24 h.

Next, we investigated the stability of crosslinked films of J51:N2200 bulk heterojunction films to withstand physical agitation using sonication (**Figure 6**). J51:N2200 films were placed in Hellendahl-type glass staining dishes, submerged in water, and sonicated for 1 h. Photographs of the films after each time interval showed significantly greater removal of non-crosslinked J51:N2200 films from the glass substrate in comparison to their crosslinked counterparts (Figure 6a). To quantify the physical damage done to each film, we used UV–vis to monitor changes in film thickness (Figure 6b and Figure S11, Supporting Information) and image analysis (i.e., color thresholding) to approximate film coverage on the substrate (Figure 6c). We found that sonicating a semiconducting polymer film results in both adhesive and cohesive damage. The photographs and subsequent image analysis show a gradual reduction in surface coverage, suggesting that the sonication resulted in adhesive failure due to the delamination of the film from the glass substrate. Moreover, for regions in which film remained, UV–vis spectra suggest that the thickness also decreased. After 1 h, the crosslinked film lost only ≈20% of the total film volume, compared to ≈90% of the non-crosslinked film.

To quantify the way in which crosslinking affects both the cohesive and adhesive properties of the films, we performed debonding tests using a double cantilever beam (DCB) setup (**Figure 7**). Both non-crosslinked and crosslinked J51:N2200 film stacks required similar amounts of energy to propagate fracture (Figure 7a), yet exhibited different debonding behavior (Figure 7b). In contrast, the PTB7-Th:N2200 film stacks fractured within the same layer (Figure 7c), while the crosslinked active layer required 5% more energy to propagate the fracture.

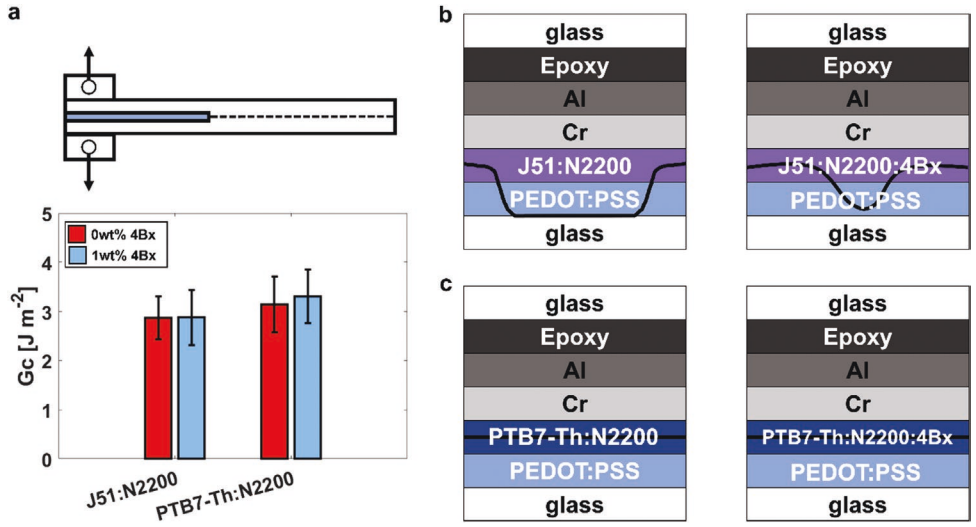

Figure 7. a) Cohesive fracture tests were conducted using double cantilever beam (DCB) measurements in order to measure the fracture energy of a glass/PEDOT:PSS/BHJ/Cr/Al stack. X-ray photoelectron spectroscopy (XPS) was conducted after fracturing DCB samples in order to determine the interface of fracture for sample stacks with non-crosslinked and crosslinked films of b) J51:N2200 and c) PTB7-Th:N2200.

XPS measurements were conducted on opposing surfaces of each sample stack after fracture to identify the interface of fracture (Figures S12 and S13, Supporting Information). For PTB7-Th:N2200, both the crosslinked and non-crosslinked films resulted in cohesive failure within the PTB7-Th:N2200 layer. In contrast, the J51:N2200 films experienced both adhesive and cohesive failure: adhesive failure at the PEDOT:PSS/J51:N2200 interface and cohesive failure within the J51:N2200 film. The adhesive failure likely occurred due to domains of J51 serving as fracture (e.g., embrittling) pathways into the PEDOT:PSS layer. When crosslinked, XPS suggested that samples with a J51:N2200:4Bx active layer primarily underwent cohesive failure within the active layer. For these J51:N2200:4Bx samples, polymer chains were crosslinked to one another, likely reducing the embrittling effect of J51 domains. Likewise, crosslinking with 4Bx increased the adhesion to the PEDOT:PSS layer (e.g., possibly due to cross-reactivity with the PEDOT:PSS interface). However, fracture still propagated through some available pathways within the bulk heterojunction, suggesting that some regions within the J51:N2200 were less crosslinked than others. Similarly, it is possible that the meandering fracture path of the non-crosslinked J51:N2200 film resulted in an increase in the measured fracture energy.[84] Therefore, the measured fracture energy between the non-crosslinked and crosslinked samples remained approximately the same. Thus, XPS suggests that crosslinking with low loadings of 4Bx reduces (but does not necessarily eliminate) the number of paths for the fracture to propagate from the polymer blend into the PEDOT:PSS (i.e., across layers). These findings validate previous experiments observing that the crosslinked J51:N2200 film showed a smaller decrease in film thickness over 1 h of sonication. Fracture tests suggest that this decreased loss can be attributed to the increase in cohesion due to the crosslinked network within the solid film (Figure 7b).

In contrast, sample stacks with both non-crosslinked and crosslinked active layers of PTB7-Th:N2200 experienced cohesive failure within the active layer. The crosslinked PTB7-Th:N2200:4Bx samples had an average G_c of ≈5% greater than the non-crosslinked PTB7-Th:N2200 samples. This difference suggests that crosslinking with 4Bx increased the cohesive strength of the PTB7-Th:N2200 active layer and possibly the adhesive strength of the PTB7-Th:N2200/PEDOT:PSS interface. However, the difference was not significant enough to change the interface of fracture. Previous work done by the O'Connor group showed that the fracture energy of an all-polymer blend is largely dictated by the tougher polymer (i.e., N2200).[73] Thus, when the fracture is unable to propagate to the PEDOT:PSS layer (as for J51:N2200), the increase in the toughness of N2200 when crosslinked (Table S1, Supporting Information) translates to an active layer that requires a greater amount of energy to propagate the fracture.

To quantify the abrasion resistance of the crosslinked bulk heterojunction films, we measured the hardness, modulus, and elastic work in compression using nanoindentation (**Figure 8**a and Figure S14, Supporting Information). These measurements showed that the polymer films increased in hardness as a function of 4Bx loading (Figure 8b), which is consistent with the increase in resilience derived from the tensile behavior (Figure 3). Compressive measurements likewise show similar changes in the elastic modulus (Figure 8c). All films of J51:N2200 (0–2 wt% 4Bx) resulted in similar moduli. In contrast, films of PTB7-Th:N2200 had similar moduli for both 0 and 1 wt% 4Bx, but a greater modulus for 2 wt% 4Bx. Similarly, the loss modulus remained constant despite increasing 4Bx loading for both J51:N2200 and PTB7-Th:N2200 (Figure S15, Supporting Information). These differences agreed with the embrittlement previously observed in the tensile behavior of PTB7-Th:N2200 relative to increasing 4Bx loading (Figure 3c). In both J51:N2200 (Figure 8d) and PTB7-Th:N2200 (Figure 8e), the elastic work measured by nanoindentation slightly increased as the crosslinker loading increased. For J51:N2200, the plastic work remained similar between 0 and 1 wt% 4Bx

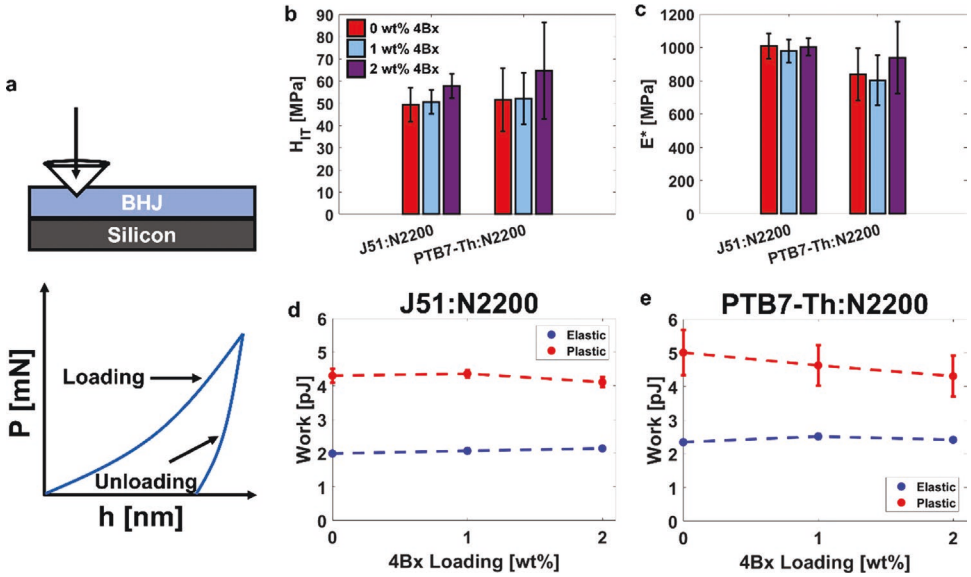

Figure 8. a) Compressive properties of J51:N2200 and PTB7-Th:N2200 with 0, 1, or 2 wt% 4Bx were measured using nanoindentation (Sinus indentation) with a Berkovich tip in order to extract the b) indentation hardness (H_{IT}) and c) elastic modulus (E^*). From the load-unloading curves, the elastic and plastic work for d) J51:N2000 and e) PTB7-Th:N2200 were extracted.

and then decreased at 2 wt% 4Bx. This compressive behavior is consistent with the tensile behavior observed in Figure 3b, in which 1 wt% 4Bx seemed to be the optimal loading for maintaining fracture strain and toughness (i.e., plastic behavior). After 1 wt% 4Bx, embrittlement resulted in a tradeoff between decreasing fracture strain and increasing tensile strength. In contrast, the plastic work continuously decreased while the elastic work monotonically increased for PTB7-Th:N2200, which is again consistent with the observed tensile behavior (Figure 3c). Due to the decreased plastic behavior, the storage modulus of PTB7-Th:N2200 increased while the loss modulus remained similar (Figure S15, Supporting Information). This change in the viscoelastic behavior resulted in a slightly lower tan δ (i.e., the ratio between loss and storage modulus) relative to increasing 4Bx loading (Figure S15, Supporting Information).

4. Conclusion

In this study, we use a four-armed azide crosslinker ("4Bx") to crosslink a library of semiconducting polymers, with special attention paid to two different bulk heterojunction films used in all-polymer solar cells (J51:N2200 and PTB7-Th:N2200). We show that 4Bx can be used to modulate the mechanical properties of these films, particularly for increasing the tensile strength, hardness, and cohesive strength. To directly probe how crosslinking affects the photovoltaic properties of the bulk heterojunction, we fabricated all-polymer solar cells. We find that crosslinked bulk heterojunctions showed significant improvements in abrasion resistance, likely in part due to the increased cohesive strength. This increased abrasion resistance translates to a more survivable device when subject to mild abrasion and scratches. Likewise, crosslinking the bulk heterojunction results in a device with increased solvent resistance (30 s of chloroform exposure) and thermal stability (> 200 h at 60 °C), but with somewhat lower performance. Nevertheless, it is our hope that devices made from conjugated polymers can be afforded greater environmental stability by simple strategies like the one explored here. In particular, solar cells with greater strength, hardness, and abrasion resistance could enable energy harvesting from surfaces subject to continuous mechanical insults.

Our work suggests the importance of investigating crosslinkers more ideally suited to conjugated polymers than is 4Bx. For example, the presence of 4Bx increases the insulating fraction of a crosslinked film relative to a pristine film. There may be an opportunity to explore conjugated crosslinkers or those which are less likely to disrupt lamellar packing within ordered domains. Thus, the rational design of both conjugated polymers and crosslinkers for the purposes of increasing the mechanical robustness could also allow for greater crosslinker loading with a reduced deleterious effect on the electronic properties.

Finally, this work focuses on a relatively small subset of conjugated polymers, most of which are structurally distinct from one another. However, systematic exploration of the effect of crosslinking should be done with the many assorted families of conjugated polymers that are widely in use today. In conjunction with structure-property studies of the crosslinker structure on the physical properties of a conjugated polymer, further studies could yield a deeper understanding of how the mechanical and electronic properties of conjugated polymers can be modified to better suit applications expected to survive rigorous environmental conditions.

Supporting Information

Supporting Information is available from the Wiley Online Library or from the author.

Acknowledgements

This work was supported by the Air Force Office of Scientific Research (AFOSR) grant no. FA9550-22-1-0454. K.C. acknowledges additional support as a Hellman Scholar and an Intel Scholar provided through the Academic Enrichment Program (AEP) at UCSD through the following awards: The Undergraduate Research Scholarship and Semiconductor Research Corporation Scholarship. R.R. acknowledges support from the National Science Foundation Graduate Research Fellowship (NSF GRFP) under grant no. DGE-1144086. The authors acknowledge the use of facilities and instrumentation supported by NSF through the UC San Diego Materials Research Science and Engineering Center (UCSD MRSEC), grant DMR-2011924. This work was performed in part at the San Diego Nanotechnology Infrastructure (SDNI) of UCSD, a member of the National Nanotechnology Coordinated Infrastructure, which is supported by the National Science Foundation (Grant ECCS-2025752). The authors thank the Department of Chemistry and Biochemistry at The University of Arizona for support of the Laboratory for Electron Spectroscopy and Surface Analysis. [Correction added 26 January 2023, after initial publication: In Figure 6a, the same film image was inadvertently used for the crosslinked and non-crosslinked films at the 5 min interval. This has been replaced so that the correct image now appears for the crosslinked film.]

Conflict of Interest

The authors declare no conflict of interest.

Data Availability Statement

The data that support the findings of this study are available in the supplementary material of this article.

Keywords

crosslinking, mechanical properties, photovoltaics, polymer coatings, semiconducting polymers

Received: September 25, 2022
Revised: October 17, 2022
Published online: December 1, 2022

[1] A. X. Chen, A. T. Kleinschmidt, K. Choudhary, D. J. Lipomi, *Chem. Mater.* **2020**, *32*, 7582.
[2] M. J. Kim, M. Lee, H. Min, S. Kim, J. Yang, H. Kweon, W. Lee, D. H. Kim, J. H. Choi, D. Y. Ryu, M. S. Kang, B. S. Kim, J. H. Cho, *Nat. Commun.* **2020**, *11*, 1520.
[3] Z. Peng, K. Xian, Y. Cui, Q. Qi, J. Liu, Y. Xu, Y. Chai, C. Yang, J. Hou, Y. Geng, L. Ye, *Adv. Mater.* **2021**, *33*, 2106732.
[4] G. J. N. Wang, A. Gasperini, Z. Bao, *Adv. Electron. Mater.* **2018**, *4*, 1700429.
[5] Y. Qian, X. Zhang, L. Xie, D. Qi, B. K. Chandran, X. Chen, W. Huang, *Adv. Mater.* **2016**, *28*, 9243.
[6] S. Savagatrup, A. D. Printz, T. F. O'Connor, A. V. Zaretski, D. J. Lipomi, *Chem. Mater.* **2014**, *26*, 3028.
[7] M. U. Ocheje, B. P. Charron, A. Nyayachavadi, S. S. E. Rondeau-Gagné, *Flexible Printed Electron.* **2017**, *2*, 43002.
[8] D. C. Kim, H. J. Shim, W. Lee, J. H. Koo, D. H. Kim, *Adv. Mater.* **2020**, *32*, 1902743.
[9] J. Han, F. Bao, D. Huang, X. Wang, C. Yang, R. Yang, X. Jian, J. Wang, X. Bao, J. Chu, *Adv. Funct. Mater.* **2020**, *30*, 2003654.
[10] M. Ashizawa, Y. Zheng, H. Tran, Z. Bao, *Prog. Polym. Sci.* **2020**, *100*, 101181.
[11] S. Zhang, Y. H. Cheng, L. Galuska, A. Roy, M. Lorenz, B. Chen, S. Luo, Y. T. Li, C. C. Hung, Z. Qian, P. B. J. S. Onge, G. T. Mason, L. Cowen, D. Zhou, S. I. Nazarenko, R. F. Storey, B. C. Schroeder, S. Rondeau-Gagné, Y. C. Chiu, X. Gu, *Adv. Funct. Mater.* **2020**, *30*, 2000663.
[12] J. Y. Oh, D. Son, T. Katsumata, Y. Lee, Y. Kim, J. Lopez, H. C. Wu, J. Kang, J. Park, X. Gu, J. Mun, N. G. J. Wang, Y. Yin, W. Cai, Y. Yun, J. B. H. Tok, Z. Bao, *Sci. Adv.* **2019**, *5*, aav3097.
[13] R. Xie, A. R. Weisen, Y. Lee, M. A. Aplan, A. M. Fenton, A. E. Masucci, F. Kempe, M. Sommer, C. W. Pester, R. H. Colby, E. D. Gomez, *Nat. Commun.* **2020**, *11*, 893.
[14] M. J. Kim, A. R. Jung, M. Lee, D. Kim, S. Ro, S. M. Jin, H. D. Nguyen, J. Yang, K. K. Lee, E. Lee, M. S. Kang, H. Kim, J. H. Choi, B. Kim, J. H. Cho, *ACS Appl. Mater. Interfaces* **2017**, *9*, 40503.
[15] Y. Zheng, M. Ashizawa, S. Zhang, J. Kang, S. Nikzad, Z. Yu, Y. Ochiai, H.-C. Wu, H. Tran, J. Mun, Y.-Q. Zheng, J. B.-H. Tok, X. Gu, Z. Bao, *Chem. Mater.* **2020**, *32*, 5700.
[16] Y. Zheng, Z. Yu, S. Zhang, X. Kong, W. Michaels, W. Wang, G. Chen, D. Liu, J. Lai, N. Prine, W. Zhang, S. Nikzad, C. B. Cooper, D. Zhong, J. Mun, Z. Zhang, J. Kang, J. B. Tok, I. Mcculloch, J. Qin, X. Gu, Z. Bao, *Nat. Commun.* **2021**, *12*, 5701.
[17] E. Dauzon, X. Sallenave, C. Plesse, F. Goubard, A. Amassian, T. D. Anthopoulos, *J. Mater. Chem. C* **2022**, *10*, 3375.
[18] Z. Wang, D. Zhang, M. Xu, J. Liu, J. He, L. Yang, Z. Li, Y. Gao, M. Shao, *Small* **2022**, *18*, 2201589.
[19] J. W. Rumer, I. McCulloch, *Mater. Today* **2015**, *18*, 425.
[20] J. W. Rumer, R. S. Ashraf, N. D. Eisenmenger, Z. Huang, I. Meager, C. B. Nielsen, B. C. Schroeder, M. L. Chabinyc, I. McCulloch, *Adv. Energy Mater.* **2015**, *5*, 5.
[21] L. Hong, H. Yao, Y. Cui, R. Yu, Y. Lin, T. Chen, Y. Xu, J. Qin, C. Hsu, Z. Ge, J. Hou, *Small* **2021**, *17*, 2101133.
[22] Y. J. Cheng, C. H. Hsieh, P. J. Li, C. S. Hsu, *Adv. Funct. Mater.* **2011**, *21*, 1723.
[23] D. Qian, Q. Xu, X. Hou, F. Wang, J. Hou, Z. Tan, *J. Polym. Sci., Part A: Polym. Chem.* **2013**, *51*, 3123.
[24] C. Lee, S. Lee, G. U. Kim, W. Lee, B. J. Kim, *Chem. Rev.* **2019**, *119*, 8028.
[25] A. Facchetti, *Mater. Today* **2013**, *16*, 123.
[26] G. Wang, F. S. Melkonyan, A. Facchetti, T. J. Marks, *Angew. Chem., Int. Ed.* **2019**, *58*, 4129.
[27] L. Zhu, M. Zhang, W. Zhong, S. Leng, G. Zhou, Y. Zou, X. Su, H. Ding, P. Gu, F. Liu, Y. Zhang, *Energy Environ. Sci.* **2021**, *14*, 4341.
[28] J. Wang, X. Zhan, *Acc. Chem. Res.* **2021**, *54*, 132.
[29] Y. Zhang, Y. Ji, Y. Zhang, W. Zhang, H. Bai, M. Du, *Adv. Funct. Mater.* **2022**, *32*, 2205115.
[30] S. Dey, *Small* **2019**, *15*, 1900134.
[31] S. E. Root, S. Savagatrup, A. D. Printz, D. Rodriquez, D. J. Lipomi, *Chem. Rev.* **2017**, *117*, 6467.
[32] H. Kang, W. Lee, J. Oh, T. Kim, C. Lee, B. J. Kim, *Acc. Chem. Res.* **2016**, *49*, 2424.
[33] Z. C. Wen, H. Yin, X. T. Hao, *Surf. Interfaces* **2021**, *23*, 100921.
[34] Q. Guo, Q. Guo, Y. Geng, A. Tang, M. Zhang, M. Du, X. Sun, E. Zhou, *Mater. Chem. Front.* **2021**, *5*, 3257.
[35] S.-C. Wu, L. T. Strover, X. Yao, X. Q. Chen, W. J. Xiao, L. N. Liu, J. Wang, I. Visoly-Fisher, E. A. Katz, W. S. Li, *ACS Appl. Mater. Interfaces* **2018**, *10*, 35430.
[36] N. Y. Kwon, S. H. Park, H. Kang, Y. U. Kim, H. D. Chau, A. K. Harit, H. Y. Woo, H. J. Yoon, M. J. Cho, D. H. Choi, *ACS Appl. Mater. Interfaces* **2021**, *13*, 16754.
[37] F. Yang, W. Zhao, Q. Zhu, C. Li, W. Ma, J. Hou, W. Li, *Macromolecules* **2019**, *52*, 2214.

[38] M. Schock, S. Bräse, *Molecules* **2020**, *25*, 1009.
[39] X. Zhao, Y. Zhao, Q. Ge, K. Butrouna, Y. Diao, K. R. Graham, J. Mei, *Macromolecules* **2016**, *49*, 2601.
[40] A. Wadsworth, H. Chen, K. J. Thorley, C. Cendra, M. Nikolka, H. Bristow, M. Moser, A. Salleo, T. D. Anthopoulos, H. Sirringhaus, I. McCulloch, *J. Am. Chem. Soc.* **2020**, *142*, 652.
[41] W. Zhang, J. Smith, S. E. Watkins, R. Gysel, M. McGehee, A. Salleo, J. Kirkpatrick, S. Ashraf, T. Anthopoulos, M. Heeney, I. McCulloch, *J. Am. Chem. Soc.* **2010**, *132*, 11437.
[42] H. S. Kim, G. Huseynova, Y. Y. Noh, D. H. Hwang, *Macromolecules* **2017**, *50*, 7550.
[43] Z. G. Zhang, Y. Yang, J. Yao, L. Xue, S. Chen, X. Li, W. Morrison, C. Yang, Y. Li, *Angew. Chem., Int. Ed.* **2017**, *56*, 13503.
[44] R. Runser, S. E. Root, D. E. Ober, K. Choudhary, A. X. Chen, C. Dhong, A. D. Urbina, D. J. Lipomi, *Chem. Mater.* **2019**, *31*, 9078.
[45] C. P. Chen, Y. Y. Tsai, Y. C. Chen, Y. H. Li, *Sol. Energy* **2018**, *176*, 170.
[46] J. H. Kim, A. Nizami, Y. Hwangbo, B. Jang, H. J. Lee, C. S. Woo, S. Hyun, T. S. Kim, *Nat. Commun.* **2013**, *4*, 2520.
[47] M. R. Vanlandingham, N. K. Chang, P. L. Drzal, C. C. White, S. H. Chang, *J. Polym. Sci., Part B: Polym. Phys.* **2005**, *43*, 1794.
[48] C. C. White, M. R. Vanlandingham, P. L. Drzal, N. K. Chang, S. H. Chang, *J. Polym. Sci., Part B: Polym. Phys.* **2005**, *43*, 1812.
[49] H. Lu, B. Wang, J. Ma, G. Huang, H. Viswanathan, *Mech. Time-Depend. Mater.* **2003**, *7*, 189.
[50] Y. Wang, L. Shang, P. Zhang, X. Yan, K. Zhang, S. Dou, J. Zhao, Y. Li, *Polym. Test.* **2020**, *83*, 106353.
[51] G. M. Odegard, T. S. Gates, H. M. Herring, *Exp. Mech.* **2005**, *45*, 130.
[52] C. Klapperich, K. Komvopoulos, L. Pruitt, *J. Tribol.* **2001**, *123*, 624.
[53] A. Chakravartula, K. Komvopoulos, *Appl. Phys. Lett.* **2006**, *88*, 28.
[54] H. Li, N. X. Randall, J. J. Vlassak, *J. Mater. Res.* **2010**, *25*, 728.
[55] S. Mahouche-Chergui, Z. Boussaboun, A. Oun, M. Kazembeyki, C. G. Hoover, B. Carbonnier, C. M. Ouellet-Plamondon, *Chem. Eng. Sci.* **2021**, *236*, 116482.
[56] W. C. Oliver, G. M. Pharr, *J. Mater. Res.* **1992**, *7*, 1564.
[57] S. E. Root, S. Savagatrup, C. J. Pais, G. Arya, D. J. Lipomi, *Macromolecules* **2016**, *49*, 2886.
[58] M. F. Kanninen, *Int. J. Fract.* **1973**, *9*, 83.
[59] N. Y. Doumon, G. Wang, X. Qiu, A. J. Minnaard, R. C. Chiechi, L. J. A. Koster, *Sci. Rep.* **2019**, *9*, 4350.
[60] A. Zusan, B. Gieseking, M. Zerson, V. Dyakonov, R. Magerle, C. Deibel, *Sci. Rep.* **2015**, *5*, 8286.
[61] S. Savagatrup, A. D. Printz, T. F. O'Connor, I. Kim, D. J. Lipomi, *Chem. Mater.* **2017**, *29*, 389.
[62] F. C. Spano, C. Silva, *Annu. Rev. Phys. Chem.* **2014**, *65*, 477.
[63] F. C. Spano, *J. Chem. Phys.* **2005**, *122*, 234701.
[64] L. Gao, Z. G. Zhang, L. Xue, J. Min, J. Zhang, Z. Wei, Y. Li, *Adv. Mater.* **2016**, *28*, 1884.
[65] K. Choudhary, A. X. Chen, G. M. Pitch, R. Runser, A. Urbina, T. J. Dunn, M. Kodur, A. T. Kleinschmidt, B. G. Wang, J. A. Bunch, D. P. Fenning, A. L. Ayzner, D. J. Lipomi, *ACS Appl. Mater. Interfaces* **2021**, *13*, 51436.
[66] Y. Zheng, G. J. N. Wang, J. Kang, M. Nikolka, H. C. Wu, H. Tran, S. Zhang, H. Yan, H. Chen, P. Y. Yuen, J. Mun, R. H. Dauskardt, I. McCulloch, J. B. H. Tok, X. Gu, Z. Bao, *Adv. Funct. Mater.* **2019**, *29*, 1905340.
[67] Q. Zhang, Z. Chen, W. Ma, Z. Xie, J. Liu, X. Yu, Y. Han, *ACS Appl. Mater. Interfaces* **2019**, *11*, 32200.
[68] X. Yi, B. Gautam, I. Constantinou, Y. Cheng, Z. Peng, E. Klump, X. Ba, C. H. Y. Ho, C. Dong, S. R. Marder, J. R. Reynolds, S. W. Tsang, H. Ade, F. So, *Adv. Funct. Mater.* **2018**, *28*, 1802702.
[69] Y. Xia, C. Musumeci, J. Bergqvist, W. Ma, F. Gao, Z. Tang, S. Bai, Y. Jin, C. Zhu, R. Kroon, C. Wang, M. R. Andersson, L. Hou, O. Inganäs, E. I. Wang, *J. Mater. Chem. A* **2016**, *4*, 3835.
[70] S. H. Park, Y. Kim, N. Y. Kwon, Y. W. Lee, H. Y. Woo, W. S. Chae, S. Park, M. J. Cho, D. H. Choi, *Adv. Sci.* **2020**, *7*, 1902470.
[71] J. Yuan, W. Guo, Y. Xia, M. J. Ford, F. Jin, D. Liu, H. Zhao, O. Inganäs, G. C. Bazan, W. Ma, *Nano Energy* **2017**, *35*, 251.
[72] A. Sharma, R. Singh, G. P. Kini, J. Hyeon Kim, M. Parashar, M. Kim, M. Kumar, J. S. Kim, J. J. Lee, *ACS Appl. Mater. Interfaces* **2021**, *13*, 7405.
[73] N. Balar, J. J. Rech, R. Henry, L. Ye, H. Ade, W. You, B. T. O'Connor, *Chem. Mater.* **2019**, *31*, 5124.
[74] T. Sun, J. I. Scott, M. Wang, R. J. Kline, G. C. Bazan, B. T. O. Connor, *Adv. Electron. Mater.* **2017**, *3*, 1600388.
[75] J. I. Scott, X. Xue, M. Wang, R. J. Kline, B. C. Hoffman, D. Dougherty, C. Zhou, G. Bazan, B. T. O'Connor, *ACS Appl. Mater. Interfaces* **2016**, *8*, 14037.
[76] X. Xu, D. Li, J. Yuan, Y. Zhou, Y. Zou, *EnergyChem* **2021**, *3*, 100046.
[77] M. Jørgensen, K. Norrman, F. C. Krebs, *Sol. Energy Mater. Sol. Cells* **2008**, *92*, 686.
[78] J. Lee, J. W. Kim, S. A. Park, S. Y. Son, K. Choi, W. Lee, M. Kim, J. Y. Kim, T. Park, *Adv. Energy Mater.* **2019**, *9*, 1901829.
[79] J. Jo, S. S. Kim, S. I. Na, B. K. Yu, D. Y. Kim, *Adv. Funct. Mater.* **2009**, *19*, 866.
[80] D. E. Motaung, G. F. Malgas, C. J. Arendse, *J. Mater. Sci.* **2011**, *46*, 4942.
[81] R. De Bettignies, J. Leroy, M. Firon, C. Sentein, *Synth. Met.* **2006**, *156*, 510.
[82] M. Modarresi, A. Mehandzhiyski, M. Fahlman, K. Tybrandt, I. Zozoulenko, *Macromolecules* **2020**, *53*, 6267.
[83] L. Bießmann, L. P. Kreuzer, T. Widmann, N. Hohn, J.-F. Moulin, *ACS Appl. Mater. Interfaces* **2018**, *10*, 9865.
[84] B. L. Watson, N. Rolston, A. D. Printz, R. H. Dauskardt, *Energy Environ. Sci.* **2017**, *10*, 2500.